Ultrasonics 94 (2019) 10–19

Contents lists available at ScienceDirect

Ultrasonics

journal homepage: www.elsevier.com/locate/ultras

Determining sodium diffusion through acoustic impedance measurements using 80 MHz Scanning Acoustic Microscopy: Agarose phantom verification

Irem Demirkan[a,*], Mehmet Burcin Unlu[a,b,c], Bukem Bilen[a]

[a] Bogazici University, Department of Physics, Istanbul 34342, Turkey
[b] Global Station for Quantum Medical Science and Engineering, Global Institution for Collaborative Research and Education (GI-CoRE), Hokkaido University, Sapporo 060-8648, Japan
[c] Department of Radiation Oncology, Stanford University School of Medicine, Stanford, CA, USA

ARTICLE INFO

Keywords:
Acoustics
Scanning Acoustic Microscope
Diffusion
Sodium

ABSTRACT

The purpose of this study is to explore the feasibility of time-dependent acoustic impedance measurement by Scanning Acoustic Microscopy (SAM) for analyzing the sodium diffusion. The purpose is motivated by the fact that sodium monitoring is challenging and still in the area of exploratory analysis despite its biological importance. To our knowledge, this is the first study in which sodium diffusion has been investigated by time-dependent acoustic impedance measurements provided by SAM. We first tested the idea in an agarose phantom as a proof-of-concept. Accordingly, we designed the agarose phantom which initially contains a well of sodium chloride (NaCl) solution moving radially into the phantom. By using NaCl diffusion in the phantom, we obtained two-dimensional (2D) acoustic impedance (Z) maps over time through SAM operating with 80 MHz ultrasonic transducer having a lateral resolution of 20 μm. A linear correlation between the changes in the concentration profile of the phantom and its acoustic impedance was introduced. Analysis of experimental data proved that spatially changing acoustic impedance could be ascribed to the diffusion process and produced a diffusion coefficient in the order of 10^{-5} cm^2/s which matches well with the literature. Our results showed that SAM could monitor the time-dependent alterations in acoustic impedance resulting from the diffusion of sodium inside the agarose phantom. With this study, SAM shows a promise as a monitoring tool not only to obtain static images but also to perform dynamic investigations of sodium ions with the advantages of providing images in micrometer resolution with a scanning time no longer than 2 min for an image area of 4.8 mm × 4.8 mm.

1. Introduction

The primary purpose of this work is to show the potential of time-varying acoustic impedance measurement provided by Scanning Acoustic Microscopy (SAM) in the analysis of sodium concentration activity. Though sodium level gives vital information about biological processes, its precise monitoring is yet under investigation. Towards, our study is the first proposing that time-dependent acoustic impedance measurements by SAM may be used to explore sodium concentration dynamics. Sodium (Na^+), being the primary cation in extracellular fluids of living beings, is known to regulate bodily functions and biological processes. It also provides vital information about physiological and pathological states. Almost all living organisms could be unified to have the ability in sustaining the difference in sodium amount between the interior and the exterior compartments of their cells. Typically, sodium concentration of the viable cell interior is around 10–15 mmol/L while sodium concentration outside the cell averages to 140–150 mmol/L [1–3]. Organisms divide a considerable portion of the metabolic energy to sustain the sodium gradient. Since, this gradient has a crucial role in nutrient intake, production and transmission of action potentials, regulation of intra- and extracellular ions, and controlling of the cell volume [1–3]. Particularly, disruptions altering the sodium ion homeostasis are known to be major hallmarks of cautious complications in cell integrity and ion homeostasis. Therefore, accurate determination and monitoring of sodium dynamics hold the key to diagnosis and prognosis of many diseases such as cancer, stroke, kidney, heart diseases and multiple sclerosis (MS) [1–3].

A number of analysis and monitoring approaches have been conducted to investigate variations in sodium content. Flame atomic emission spectroscopy, atomic absorption, flow cytometry, ion-selective electrode (ISE) and neutron activation are some of the sodium assay techniques [4–6]. However, these methods may be harmful to

* Corresponding author.
E-mail address: irem.demirkan@boun.edu.tr (I. Demirkan).

https://doi.org/10.1016/j.ultras.2018.12.013
Received 23 October 2018; Received in revised form 22 December 2018; Accepted 22 December 2018
Available online 26 December 2018
0041-624X/

biological samples like tissues, cell cultures, serum and urine when time duration is considered. Besides, they are far from being practical because of the fact that they lack actual quantifications, sufficient spatial resolution, interference-free and simple operating principles. Moreover, Sodium Magnetic Resonance Imaging (sodium MRI) offers visualization of the dynamic and static monitoring of sodium [7–9]. However, although being a non-destructive and reliable method, low sodium concentration of tissues or cell populations (i.e cell interior 10–15 mmol/L and cell exterior 140–150 mmol/L) leads to limitations including low resolution (2–10 mm), low signal-to-noise ratio (around 20–40), long scanning times (10–30 min), which impede studies on exact sodium monitoring [9]. Also, this technique necessitates a compact tissue in a magnetic space. The current methods used to image or monitor sodium concentration within the biological surrounding have constraints and improvement is required for precise and reliable quantification. Therefore, further research is necessary to obtain direct, precise, sensitive/specific, simple analysis and monitoring of sodium level as well as improving current techniques. Acoustic measurement by Scanning Acoustic Microscopy (SAM), which uses high-frequency sound waves (80–400 MHz) to map elastic properties of the sample through the measurements of acoustic impedance and sound speed at microscopic levels without adverse mechanical effects [10], may be an alternative to these investigation tools. Since, in comparison to the previously mentioned techniques, it has the benefits of micrometer resolution, direct non-destructive monitoring capability, no requirement of a special sampling process, quick measurement (i.e 2 min for 4.8 mm × 4.8 mm target) with an easy application [10] and applicability to bulk tissues [11–15] as well as to cell populations [16–20]. Thus far, SAM has been applied to determine the elastic features of live cell populations and tissues through the measurements of acoustic impedance and sound speed [11–20]; and it has never been used to image and monitor the sodium concentration activity. We claim that SAM may also be successful in quantifying sodium concentration activity by means of time-dependent acoustic impedance measurements and it can offer much more practical determination than the above methods.

In this study, we reported the first use of SAM with time-dependent acoustic impedance measurements to investigate the diffusion of sodium within the agarose phantom model and the study is organized as follows: Section 1 is the introduction part encompassing general information about the importance of sodium in biology, its monitoring, the related SAM literature and the purpose of our study. Section 2 outlines the method and analysis with subsections as follows: Phantom design and sample preparation, the theory of diffusion process, principles of SAM and the theory of acoustic impedance measurement. Section 3 gives the experimental outcomes. Section 4 and 5 present the discussion and conclusion of the study, respectively.

2. Method and analysis

2.1. Phantom design and sample preparation

Agarose phantom is imaging specimen of known acoustic properties such as sound speed and acoustic attenuation coefficient and facilitates and quickens the development of the imaging systems with its easy preparation protocol and reasonable cost [21]. In light of all these, the ability of SAM in sodium content determination and monitoring was first tested in the agarose phantom before investigating the ability of SAM in biological surroundings such as live cell populations or tissues and serum. We prepared an agarose phantom using commercial agar powder and distilled water. We fixed the concentration at 2% (weight of agar powder (g)/100 ml distilled water) (w/v). The swirled mixture of agar and distilled water was boiled up to a temperature changing between 80–90 °C. When the mixture cooled down to 70 °C, we poured it into the polystyrene petri dishes of diameter 4 cm and 8 cm and let it cool further down to room temperature (25 ± 1 C°). The mixture was poured as a thin layer of thickness of 1 cm within the petri dishes for neglecting the effects of gravity. Note that, in the presence of an external force, such as gravitational force, it becomes harder to describe the diffusion of NaCl solution in the agarose phantom by the well-known Fick's law [22].

The range of physiological sodium concentration is limited, but disruptions affecting the ion balance may result in increases in the sodium level within the biological medium. Accordingly, we specified the range, which covers physiologically possible sodium content within biological mediums, between 130 and 350 mmol/L. The values of agarose/saline test phantoms of known sodium concentration were also considered [9]. The NaCl solution concentration C is defined in units of g/100 ml (w/v). In terms of percentages, the biologically possible sodium amounts correspond to the range of 0.8–2%. First of all, to get the general trend, we prepared low concentrations NaCl changing from 0.8% to 2% with increments of 0.2% and high concentrations ranging from 2% to 5% with increases of 1%. In the second part, 10% NaCl was prepared to quantify sodium diffusion within the agarose phantom for time durations in the order of hours (i.e. 1-h) to give a better view of the study. Acoustic impedance values change ranging from 0.8% to 10% were quantified and the acoustic impedance values against previously mentioned sodium concentrations were plotted to illustrate the relationship.

We created a well of diameter of 7 mm in the polystyrene petri dish of diameter 4 cm, to deposit and liberate NaCl solution of a concentration within the biological range (130–350 mmol/L) [9]. The diameter of the dish for biologically possible sodium concentrations was selected because of the reason that the concentration gradient between the phantom (background) and the well leads to diffusion to be observed within a period of time in the order of minutes (i.e. 15 min). Then, we prepared another phantom inside the petri dish of diameter 8 cm with a well of diameter of 14 mm to track very high total sodium content (i.e. 10%), which is not in the possible physiological range but induces diffusion process to be observed for a time span of hours (i.e. 1-h). For both agarose set-ups, we used a dropper to pour a fixed volume of NaCl solution of any concentration into the well. Side and top views of the agarose phantoms structured for visualizing the sodium motility characteristics are shown in Fig. 1.

The total amount of NaCl solutions tested in this study remained constant through diffusion process, as indicated in Eq. (1)

$$\int_{phantom} Cdv = constant. \tag{1}$$

where C refers to the NaCl concentration in units of g/100 ml. We used the measurements of acoustic impedance at time intervals of 2 min to image and verify the diffusion of sodium ion in the agarose phantom.

2.2. Theory of diffusion process

Diffusion in a homogeneous medium is defined by Fick's first law, which relates the diffusive flux F to the concentration gradient as

$$\boldsymbol{F} = -D \cdot \nabla C, \tag{2}$$

where C is the concentration of the diffusing substance and D is the diffusion coefficient. It describes diffusion as a flow of substance resulting from the concentration gradient between mediums. As shown in Fig. 1, the agarose phantoms initially included two concentric regions: A well and the background. The well was filled with NaCl. NaCl diffuses from its nest to the background due to the concentration gradient. The diffusion of NaCl in the agarose phantom follows the Fick's second law which states the change in concentration with time as given

$$\frac{\partial C}{\partial t} = \nabla \cdot (D \nabla C), \tag{3}$$

where t refers to time. There was no varying concentration along the z-direction within the agarose phantoms because of its structure. Therefore, we assumed that diffusion could be investigated in 2-dimensions

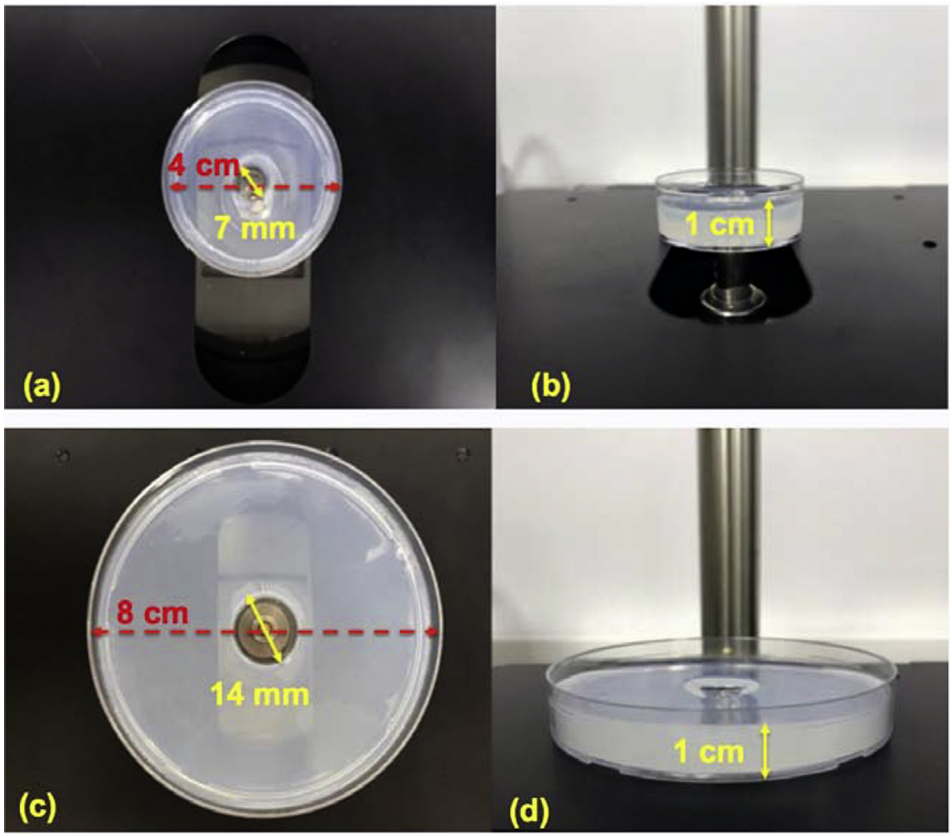

Fig. 1. (a) Lateral and (b) top perspectives of agarose phantom of diameter 4 cm, (c) lateral and (d) top perspectives of agarose phantom of diameter 8 cm. The concentric wells of NaCl solutions are 7 mm (a) and 14 mm (c).

(2D). Eq. (3) can be solved using the separation of variables method for a disc of radius a on an infinite plane surface. The corresponding result gives concentration C at radius r and time t as

$$C(r,t) = \frac{C_i}{2Dt}\exp\left(\frac{-r^2}{4Dt}\right)\int_0^a \exp\left(\frac{-r'^2}{4Dt}\right) I_0\left(\frac{rr'}{2Dt}\right) r'dr' \tag{4}$$

in which C_i refers to the initial concentration of the disc, t is time and I_0 is the modified Bessel function of the first kind of zeroth order. When $t > 0$, the maximum concentration of NaCl is observed at the disc's center, and this equation can be reduced to [23,24]

$$C = C_i\left(1 - \exp\left(\frac{-a^2}{4Dt}\right)\right). \tag{5}$$

with the aim of defining the diffusion of substances into large volumes.

2.3. Scanning Acoustic Microscopy

Here, we proposed a novel technique to quantify the diffusion of sodium ions into agarose phantom by time-dependent acoustic impedance monitoring at room temperature (25 ± 1C°). We performed all measurements with SAM. A photograph of the SAM system is shown in Fig. 2.

SAM is a non-invasive and easy-to-operate technique capable of detecting variations in elastic features of samples under investigation. SAM can measure and map microstructure of the sample as alterations in sound speed and acoustic impedance profiles with no requirement of dyeing process. In SAM, an acoustic wave is generated by a piezoelectric transducer and focused onto a sample by a sapphire lens; then it is reflected and received by the same transducer. The intensity image of the reflection, which depends on the features of the sample, is transformed into the acoustic impedance of the sample or the speed of sound passing through the sample. 2D images at the microscopic level are produced by mechanically scanning the transducer along the X-Y axes below the sample. Regarding the characteristics of the sample (tissue or cell), the resolution of the system can be improved by changing the frequency of the transducer. Namely, as the frequency of the transducer increases, the spatial resolution will enhance [10,25,26].

Fig. 3 illustrates a schematic diagram and two different measurement modes of SAM. SAM has two different measurement modes; speed of sound and acoustic impedance. The relationship between the sound speed value and elastic bulk modulus of a fluid-like medium is defined as $c = \sqrt{K/\rho}$, where c is the sound speed, K is the elastic bulk modulus, and ρ is the density [10,25]. In sound speed mode, an approximately 10 μm thick flat cross-section of a specimen placed on a substrate is in contact with distilled water, which is introduced between the transducer and the sample to improve coupling. Reflections from the substrate and the specimen are collected to plot the speed of sound passing through the specimen. In acoustic impedance measurement mode, cross-sections of samples can be observed without unique slicing and staining processes, but the front surface of the sample must be as flat as possible to retain substrate-surface attachment properly. The acoustic impedance Z is defined as the product of the density ρ and sound speed c and reflects the elasticity of the target and is formulated as $Z = \rho c$ [10,25].

In the present study, a SAM system (modified AMS-50SI, Honda Electronics CO., Ltd, Japan), equipped with a transducer having 80 MHz center frequency, was tested in following the acoustic impedance changes induced by sodium ion diffusion within the agarose phantom over time. Accordingly, the system was operated in the acoustic impedance measurement mode. Here, 80 MHz transducer was selected due to the adequate resolution required for monitoring the cumulative motility, namely, displacement of the NaCl solution [27]. The lateral resolution of 80 MHz transducer was 20 μm. 80 MHz

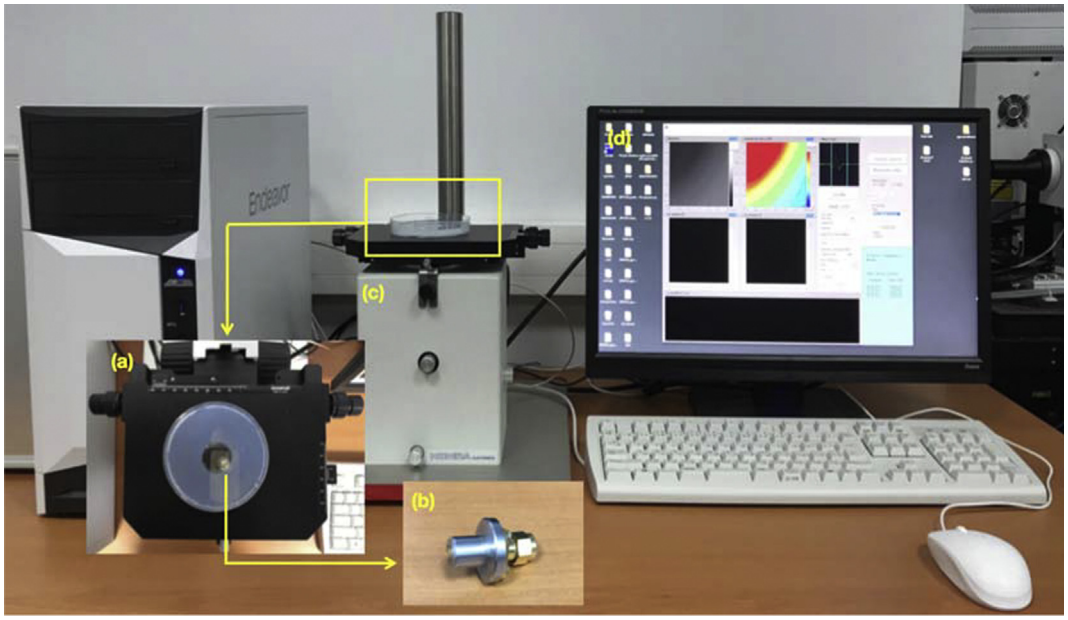

Fig. 2. Scanning acoustic microscopy system in our laboratory. (a) Top view of the agarose phantom and the well used for monitoring NaCl diffusion, (b) 80 MHz transducer (PVDF-TrFE), (c) X-Y stage and (d) computer display.

transducer, which had a PVDF-TrFE membrane, had a spot size of 17 μm and a focal length of 1.5 mm. 2D maps of samples were obtained by scanning the transducer placed on the X-Y stage. The polystyrene petri-dish filled with agarose phantom was positioned on the X-Y stage for each experiment. To raise impedance matching, we introduced a distilled water droplet (c = 1480 m/s, ρ = 1000 kg/mm^3) as a coupling liquid between the substrate and the transducer. Radio-frequency (RF) echo signals were received by the same transducer and acoustic impedance maps with 300 × 300 points were formed and plotted. The acoustic impedance data were then processed to analyze the diffusivity of sodium within agarose phantom. The maximum field of view (FOV) of the 2D maps of acoustic impedance was 4.8 mm × 4.8 mm, which has a scan increment of 16 μm. Scanning of the phantom in all experiments took about 2 min.

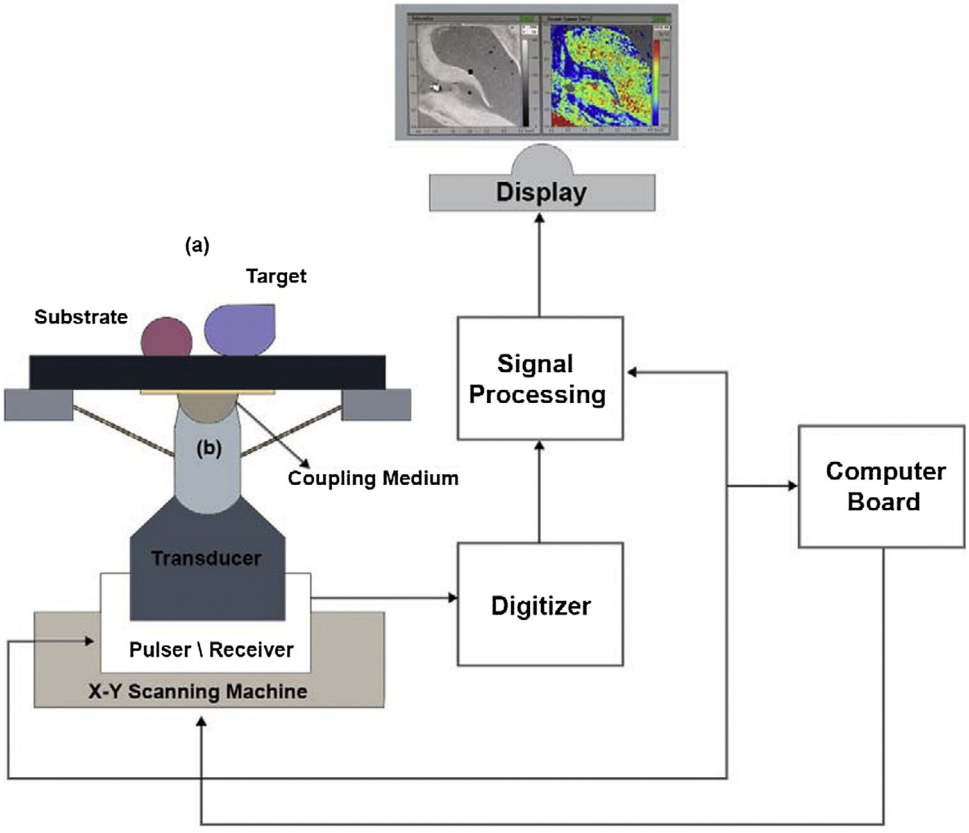

Fig. 3. Schematic diagram of SAM consisting of five parts: Transducer, X-Y scanning machine, signal processor, digitizer and display unit for monitoring. (a) Acoustic Impedance measurement mode and (b) Sound Speed measurement Mode..

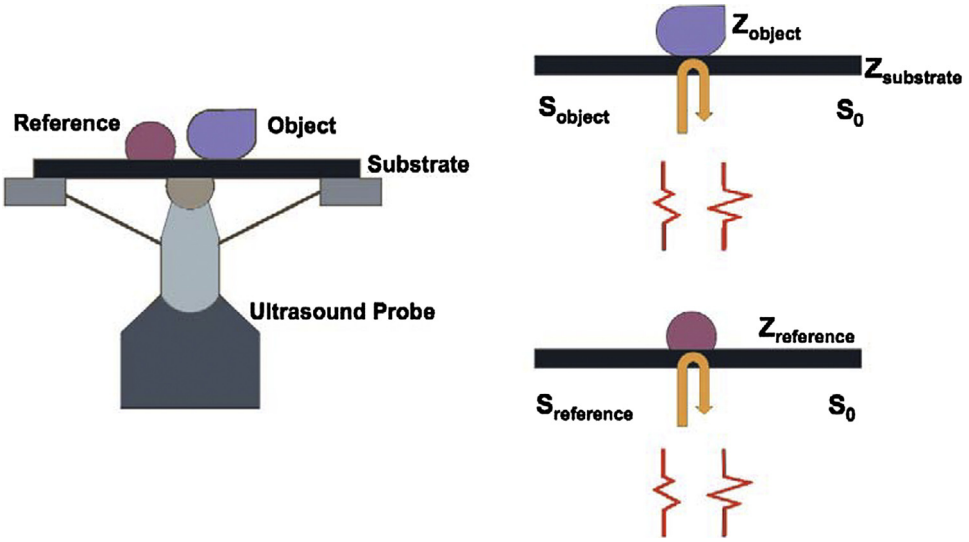

Fig. 4. Illustration of acoustic impedance measurement mode. S_0 is the transmitted signal, S_{object} is the signal reflected from the object, $S_{reference}$ is the signal reflected from the reference and Z_{object}, $Z_{substrate}$, $Z_{reference}$ are the acoustic impedances of the object, substrate and reference, respectively.

2.4. Theory of acoustic impedance measurement mode

Fig. 4 demonstrates the acoustic impedance measurement in SAM. In this study, the acoustic impedance of distilled water and polystyrene substrates were measured as 1.5×10^6 N·s/m^3 and 2.37×10^6 N·s/m^3, respectively.

In the acoustic impedance measurement mode, the signal received from the object is compared with the reference signal. The acoustic impedance image is formed from the reflected signal intensity map of the sample [12]. The reflected signal amplitude from the object under investigation S_{object} is formulated as

$$S_{object} = \frac{Z_{object} - Z_{substrate}}{Z_{object} + Z_{substrate}} S_0, \tag{6}$$

where S_0 is the transmitted signal from the ultrasound probe, Z_{object} is the acoustic impedance of the object, and $Z_{substrate}$ is the acoustic impedance of the substrate. The reference signal amplitude is formulated as in the following

$$S_{reference} = \frac{Z_{reference} - Z_{substrate}}{Z_{reference} + Z_{substrate}} S_0, \tag{7}$$

where $Z_{reference}$ accounts for the acoustic impedance of the used reference material. S_{object} and $S_{reference}$ are both directly measurable variables, however, S_0 is not. During data recording, the transmitted signal from ultrasound probe S_0 is accepted to have no alteration, then the acoustic impedance of the object can be written as

$$Z_{object} = \frac{1 - \frac{S_{object}}{S_0}}{1 + \frac{S_{object}}{S_0}} Z_{substrate} = \frac{1 - \frac{S_{object}(Z_{substrate} - Z_{reference})}{S_{reference}(Z_{substrate} + Z_{reference})}}{1 + \frac{S_{object}(Z_{substrate} - Z_{reference})}{S_{reference}(Z_{substrate} + Z_{reference})}} Z_{substrate} \tag{8}$$

The acoustic impedance maps of the objects are plotted on a display by applying the before-mentioned theory for each dataset.

3. Results

In our study, we showed the suitability of SAM system operating at 80 MHz with a lateral resolution of 20 μm in monitoring sodium ion concentration through time-varying acoustic impedance measurements in the agarose phantom. Before investigating the random behavior of sodium ions within the agarose phantom, we measured acoustic impedance values of the phantom and NaCl solutions separately. The acoustic impedance of the 2% agarose phantom was measured as $(1.52\pm0.04)\times10^6$ N·s/m^3, which was in agreement with the value obtained in a previous study [28]. We used polystyrene petri-dishes of diameters 4 cm and 8 cm to place agarose phantom for collecting reflected ultrasound signals properly during the measurements. Since, they have good hydrophilic features necessary for substrate-sample attachment.

We prepared the NaCl concentrations in and around the acceptable range of sodium content (130–350 mmol/L) regarding biological surroundings [9], therefore, the detection and monitoring the concentrations of NaCl ranging from 0.8% to 2% (g/100 ml water) were much more meaningful for the aimed study. SAM was able to measure acoustic impedances of NaCl with concentrations varying from 0.8% to 10% (g/100 ml water). Low concentrations ranging from 0.8% to 2% with increments of 0.2%, high concentrations ranging from 2% to 5% with increments of 1% and highest concentration of 10% were chosen to present the ability of SAM in quantification of sodium diffusion. Fig. 5 illustrates the experimentally recorded acoustic impedance values for the adjusted sodium chloride concentrations.

A linear relationship between acoustic impedance and concentration of NaCl solutions was extracted within this range as follows

$$Z = AC + B \tag{9}$$

in which the acoustic impedance Z is defined in units of N·s/m^3, the NaCl solution concentration C is given in units of g/100 ml water. Constants A and B were found as 0.015 and 1.513, respectively.

In Fig. 6, we showed acoustic impedance images of the 2% agarose phantom with diffusing NaCl solutions at concentrations of 1%, 1.5% and 2%, respectively. The acoustic impedances of these solutions were measured as $(1.528\pm0.0036)\times10^6$ N·s/m^3, $(1.539\pm0.003)\times10^6$ N·s/m^3 and $(1.548\pm0.0023)\times10^6$ N·s/m^3. The diffusion for 1% NaCl could be monitored for approximately 14 min, since, clear contrasts between areas of sodium contents and the background vanished quickly after the diffusion started. Herewith, for the selected concentrations, time period of 14 min was chosen for comparing the images. Acquisition of each 2D acoustic impedance microscopic image took about 2 min with 300×300 sampling points. FOV was set to 4.8 mm × 4.8 mm for each image.

In order to see clearly the diffusion mechanics within the agarose phantom and avoid data fluctuations observed in lower concentrations (1%, 1.5% and 2%), we also prepared 10% NaCl solution which is above the biologically relevant range and measured that the acoustic impedance was $(1.67\pm0.01)\times10^6$ N·s/m^3. Diffusivity of 10% NaCl solution was dynamically resolved by capturing acoustic impedance

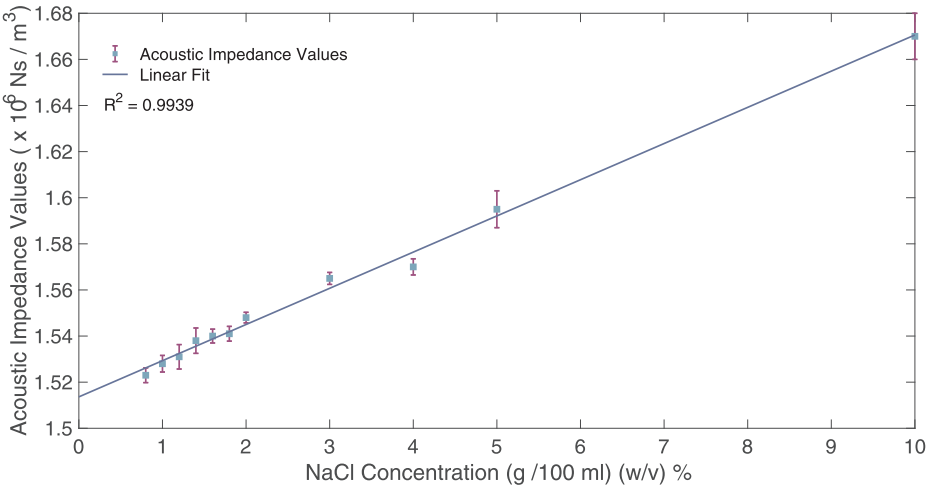

Fig. 5. Acoustic impedance values of NaCl solutions as a function of sodium content..

images every 2 min at 25 ± 1 °C till the agarose phantom and NaCl solution became isotonic, as shown in Fig. 7. Real-time screening of diffusion by SAM was achieved through observing local variations in the acoustic impedance values in the agarose phantom. As can be realized in subsequent images of the diffusion process in Fig. 7, the NaCl solution was spreading radially into the agarose phantom.

Fig. 8 reflects the changes in acoustic impedance values of the phantoms resulting from 10% NaCl solution diffusion for selected time points. Multi-colored acoustic impedance images recorded by SAM were converted to gray-scale intensity images using MATLAB and alterations in acoustic impedance values with time and position were extracted from those gray scale images as shown in Fig. 8. Moreover, acoustic impedance values inside the well, at the well-phantom border and within the 2% agarose phantom were demonstrated as an inset in Fig. 8. Trends reflecting the alterations in the acoustic impedance values for each time point were confirmed by literature findings for the NaCl diffusion within the agarose phantom. For 10% NaCl, the diffusion process was followed for 1-h timespan, however, approximately after 30 min, differences in acoustic impedances between NaCl regions, the phantom and the well-phantom border became less distinct due to the previously diffused ions and made the recording of the acoustic impedance images challenging. The acoustic impedance for time points was projected at every 10 points to increase the visibility of the data points.

The total amount of NaCl solution diffusing from its nest into the phantom was kept constant in all experiments. We used this constraint which was previously defined in Eq. (1) for scaling of the maximum acoustic impedance values of 10% NaCl solution at selected time points within the region of interest of 4.8 mm × 4.8 mm, and then fitted to Eq. (5) by means of Custom Equation Fit in MATLAB [24]. Fig. 9 reflects all measured data points throughout the experiment from the time point of four minutes to thirty-two minutes at time intervals of 2 min together with theoretical trend using Eq. (5). The maximum acoustic impedance value for each time point appeared to coincide with the theoretical fit. In course of time, they declined as expected from the diffusion. From the results of this study, it seems reasonable to conclude that spatially altering acoustic impedance values were in agreement with the diffusion process. We also extracted an experimental diffusion coefficient as 1.01×10^{-5} cm^2/s.

4. Discussion

In this study, we proposed time-dependent acoustic impedance imaging of sodium diffusion by SAM operating at 80 MHz with a lateral resolution of 20 μm. The suitability of SAM in sodium diffusion quantification was first tested within the agarose phantom as a proof-of-concept. Previous researchers have documented that imaging of sodium ion has a high potential to obtain characteristic information of disease-related variances about biological surroundings such as tissues, cells and body fluids. The normal intracellular sodium concentration of tissues is about 10 to 15 mmol/L, while extracellular sodium concentration is around 140–150 mmol/L. The range for the physiologically

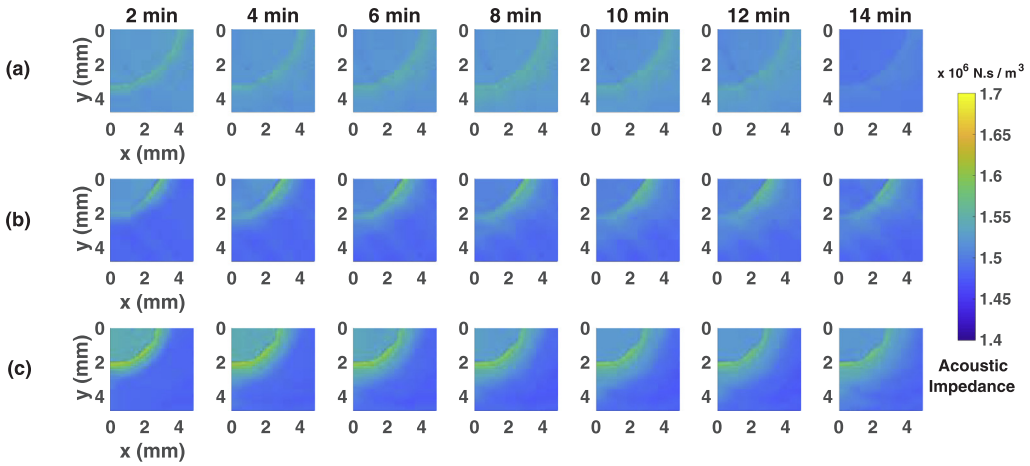

Fig. 6. Successively obtained acoustic impedance maps of the 2% agarose phantom with diffusing NaCl solutions of concentrations of (a) 1%, (b) 1.5% and (c) 2%, in 14 min. The field of view was adjusted to 4.8 mm × 4.8 mm, covered by 300 × 300 pixels.

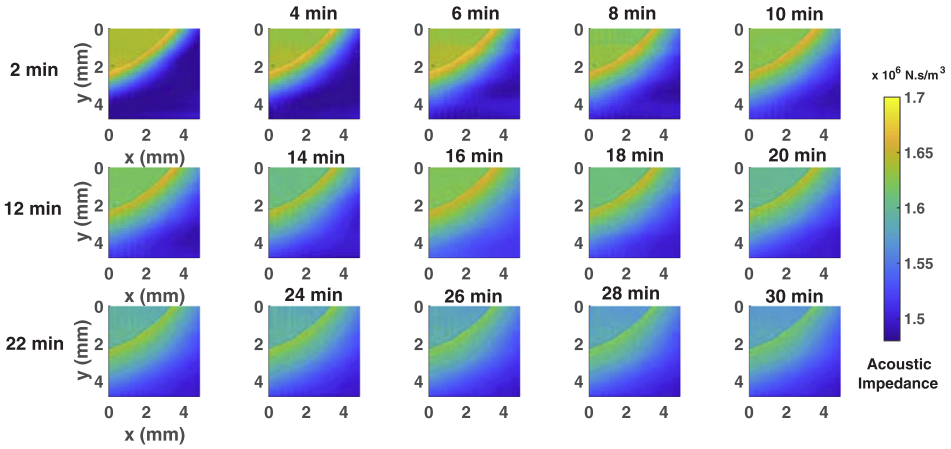

Fig. 7. Subsequent images of acoustic impedance maps of the 2% agarose phantom with diffusing 10% NaCl solution. The field of view for each image was adjusted to 4.8 mm × 4.8 mm, covered by 300 × 300 pixels.

possible sodium concentration is limited, however, researchers noted that disruptions affecting the sodium ion homeostasis can lead to increases in the sodium level within the biological media [29–33]. Besides, the agarose/saline test phantoms for sodium quantification in sodium MRI were taken into account [9]. Therefore, in this study, considering the range of the physiological sodium concentration and the reference phantoms for sodium quantification in sodium MRI, we specified the sodium concentrations in and around the physiologically possible domain of sodium amount (130–350 mmol/L) within tissues (i.e brain, muscle and cartilage) [9]. Additionally, in our study, the monitoring of sodium dynamics by SAM was first performed within the agarose phantom as proof-of-concept, since agarose phantom is a tissue-equivalent material of known acoustic features (i.e. speed of sound and acoustic attenuation coefficient) in ultrasound imaging. Also, its practical handling and easy preparation simplify and speed up the development of a system by decreasing the necessity of conducting human and animal experiment [21]. We determined the concentration of the agarose phantom at 2% for all the measurements in the study.

As well as the biologically meaningful range for the sodium concentration, we also studied the very high total sodium content of 10% which allowed us to study and verify diffusion of sodium ions through time-varying acoustic impedance measurements by SAM. Since variations along the gradient were more pronounced, the effects of fluctuations were less significant in data. Thus, this part of the study provided much more precise information than lower concentration solutions (0.8–2%) to clearly see and quantify the sodium diffusion. We parenthetically remarked that the low concentration detections of NaCl from 0.8% to 2% were more critical with our technique. Thus, in the first part of our study, we prepared NaCl concentrations ranging from 0.8% to 2% with increments of 0.2% to test the ability of SAM in low concentration saline solution measurements. Then, to get a general trend, acoustic impedance values as a function of the NaCl concentrations varying from 0.8% to 2% with increases of 0.2%, 2% to 5% with increments of 1% and 10% were obtained by SAM. Fig. 5 shows the plot of acoustic impedance values for NaCl solutions at previously defined concentrations. In the projected concentration domain in Fig. 5, we found a linear correlation between concentration and acoustic impedance which is given in Eq. (9). From the results, we concluded that the lowest concentration value for imaging and monitoring of the diffusion process by SAM functioning with 80 MHz transducer was equal to 1%. Throughout screening of the test phantom, we needed only acoustic impedance differences to track sodium ion dynamics. Namely, contrasts between the well and the agarose phantom regarding acoustic impedances were accurately imaged for the lowest saline solution concentration of 1%.

In this study, the diffusion process could be thoroughly followed for a time span of 14 min with the lowest NaCl concentration of 1%. Reductions of differences in acoustic impedances between the well and the phantom caused a decrease in the contrasts of two regions. After 14 min, the phantom was sufficiently saturated by saline solution as shown in Fig. 6. Besides, Fig. 6 shows a gallery of acoustic impedance images for 1%, 1.5% and 2% NaCl solutions recorded over a time span of 14 min to provide a comparison. Differences in acoustic impedance between the well and the background were sufficient to discern the

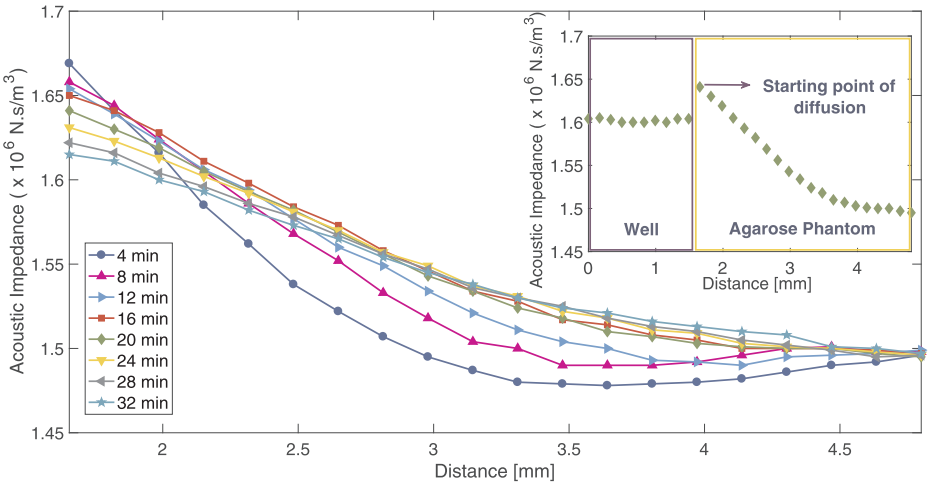

Fig. 8. Comparison of changes in acoustic impedance values of the 2% phantom resulting from 10% NaCl solution diffusion for selected time points. Initial data points correspond to the acoustic impedance values at the well-phantom border. Acoustic impedance values inside the well, at the well-phantom border and within the phantom are demonstrated in figure inset.

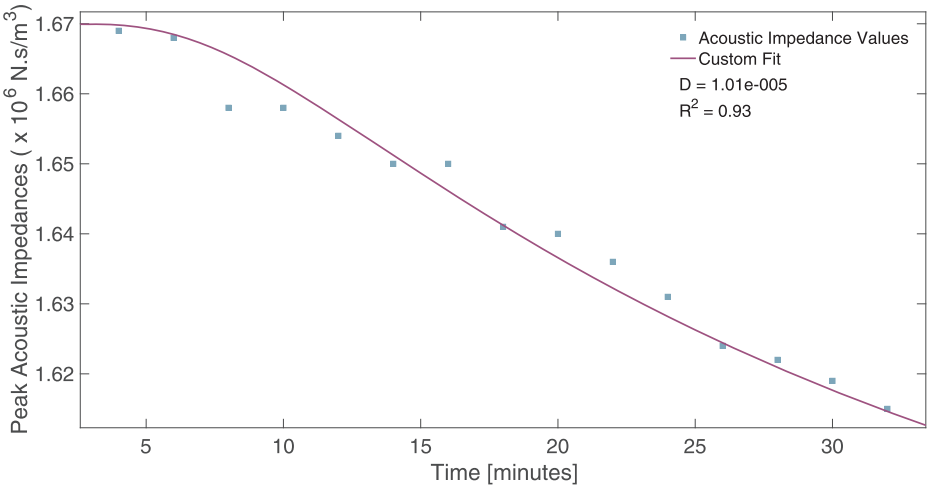

Fig. 9. Decay trends of the maximum acoustic impedance values for 10% NaCl diffusion in the 2% agarose phantom. Experimentally obtained values illustrated by the green squares were fitted to (5) producing solid line. (For interpretation of the references to colour in this figure legend, the reader is referred to the web version of this article.)

well-agarose phantom boundary and ion diffusion for low concentrations (1%, 1.5% and 2%) in the time span of 14 min. With this, SAM permitted us to follow time-dependent variations in acoustic impedance resulting from sodium concentration activity within the agarose phantom with micrometer resolution at the concentration values adjusted in the research.

The acoustic impedance of 10% NaCl, which is relatively high concentration concerning its bio-availability, was measured as $(1.67 \pm 0.01) \times 10^6$ N·s/m^3 by SAM. Compared to the NaCl concentrations of 1%, 1.5% and 2%, we obtained sharper contrasts between the well and the phantom for approximately 30 min because of the significant concentration gradient between regions initially. Fig. 7 shows acoustic images for 10% NaCl solution at consecutive times covering 30 min by acquisition step of 2 min. Acquisition of each 2D acoustic impedance image lasted in 2 min with 300 × 300 sampling points over an area of 4.8 mm × 4.8 mm. For the initial state of the experiment, a well-agarose phantom border was precisely distinguishable on acoustic impedance images for 10% NaCl solution. Due to sodium ion movements, the contrast started to fade out and border became less detectable because acoustic impedance values of both regions began to have closer values. After approximately 30 min, little contrast between the well and the phantom was observed. For 10% NaCl, we plotted acoustic impedance values as a function of position within the agarose phantom at consecutive times, as shown in Fig. 8. The acoustic impedance data were analyzed from the time point of four minutes to damp out any source of undesired perturbations such as the effect of initial velocity which can result from the introduction of NaCl solution to the well. The data recording might be initiated at any instant, however, pure diffusivity will not be observed in time periods prior to four minutes [34]. Before introducing NaCl solution into the well, the acoustic impedance of the agarose phantom was measured as $(1.52 \pm 0.04) \times 10^6$ N·s/m^3. When the 10% NaCl solution was poured into the well, the sodium concentration, and likewise the acoustic impedance of the phantom linearly increased as reported in the study of Bhatnagar *et al.* [35]. The theory of diffusion states that with instantaneous sources, the diffusion process is not continuous but terminates [23]. As shown in Fig. 8, experimentally obtained maximum acoustic impedance values within the region of interest of 4.8 mm × 4.8 mm were correlated with the theory of diffusion for instantaneous sources and exhibited similar decaying behavior at time intervals of 4 min. Over time, the acoustic impedance values monotonically decreased with distance from the well-phantom border due to the decreasing amount of NaCl solution at a particular position [23]. At the beginning of the experiment, the gradient between the acoustic impedance values of the well and the phantom was maximum, and accordingly, the curve showed a steep declination, which was due to the implementation of highly concentrated 10% NaCl solution. With increasing time, the gradient became less distinct compared to the initial trend due to previously located ions from the well into the phantom, and the curve became shallower. This was the expected trend for diffusion. We also observed fluctuations for some data points as a result of the composite gel structure of the agarose phantom. According to the study of Muhr and Blanshard [36], the structure of agarose gel was explained as a mesh, with water-filled spaces between polymer chains. Therefore, heterogeneous structure and impermeable vacancies of agarose phantom may result in unexpected acoustic impedance values. Moreover, as clearly seen in Fig. 8, it did not change the general behavior of pure diffusion.

To quantify the diffusion for 10% NaCl solution within the 2% agarose phantom, using Eq. (1), the empirically defined maximum acoustic impedance values for an image area of 4.8 mm × 4.8 mm were scaled and fitted to Eq. (5) by Custom Equation Fitting Toolbox in MATLAB. Fig. 9 shows the measured data points together with the theoretically plotted curve. The experimental acoustic impedance values were in agreement with the theoretical curve. As time elapsed, the maximum acoustic impedance values for each time point within the field of view of 4.8 mm × 4.8 mm decreased, as expected from the diffusion. We extracted a diffusion coefficient of 1.01×10^{-5} cm^2/s from Fig. 9. In the study of Schantz et al. [37], NaCl diffusion was analyzed within approximately 1.5% agarose phantom. They used a 2 g of agar powder for 100 ml water, but also stated that because of moisture in the phantom, the actual concentration was almost equal to 1.5%. The diffusion coefficient in our study was calculated to be on the order of 10^{-5} cm^2/s, which agrees with the diffusion coefficient previously reported by Schantz *et al.* [37]. Therefore, we can conclude that time-varying acoustic impedance determination by SAM is a valid method to substantiate the sodium diffusion within the agarose phantom.

As a future work, we plan on monitoring the sodium activity within the concentration range of cell interior (10–15 mmol/L) [1], which would help to distinguish intracellular and extracellular chambers and offer information about the intracellular environment. Moreover, in our work, we conducted all the experiments within the diffusion phantom since fresh tissue and cell culture investigations were not subject to this study. Before performing the sodium imaging in live tissues and cells by SAM, we first tested our idea in the agarose phantom to check whether time-dependent acoustic impedance measurements of NaCl diffusion by SAM is valid or not. Hence, our first goal for this investigation was to show and prove the ability of SAM in sodium ion dynamics monitoring by time-dependent acoustic impedance measurements within the agarose phantom which has been used as a tissue substitute in ultrasound imaging for a long time [21]. One of the reasons why we chose the agarose phantom was that agarose phantoms have been used in ultrasound imaging for a long time for the development and

characterization of the imaging systems and algorithms alongside its practical handling and easy preparation [21]. Secondly, there are similar studies in literature in which agar phantom was used to study sodium ion monitoring. For example, using agarose gel phantom and NaCl diffusion, similar experiment was conducted by using magnetic resonance electrical impedance tomography (MREIT) [24]. Thus, agarose phantom set-up was the first design that we planned for monitoring of sodium ion dynamics by SAM. On the other hand, visualization of sodium by SAM in complex surroundings such as *ex vivo* tissues and *in vitro* cell populations will be challenging due to the non-homogeneous nature of them. Yet, through considering both the similarity of the agarose phantom to tissues and our findings, we believe that one may get similar behavior for the acoustic impedance and concentration relationship as given in Fig. 5 within the intricate biological media (i.e. tissues or cell populations), as well; but this necessitates a well-thought design, optimization of the experimental conditions and specific analysis of the experimental data for the extraction of sodium ion dynamics. To illustrate, these cases, particularly cell population and serum studies, may require higher frequency ultrasonic transducers of >320 MHz which could provide the resolution that is capable of cellular imaging (i.e. around 5 μm at 320 MHz). Future studies, which take these conditions into account, will be designed for determination and monitoring of sodium ion dynamics in the biological environment.

As was pointed out in the introduction of this study, several techniques have been applied to the measurement of sodium level such as flame photometry, atomic absorption spectrophotometry, flow cytometry, ion selective electrode and neutron activation [4–8]. However, in spite of their reasonable ability to determine sodium level, all these options have quite a few shortcomings which may affect clinical applications adversely. These shortcomings comprise inadequate accuracy, indirect measurement, destructive to the integrity of the sample under investigation, laborious sampling and complicated machinery. In addition, Sodium MRI offers non-invasive quantification of sodium content [9], but demands compact tissues in a magnetic field and long scanning time (10–30 min). The low physiological amount of intra and extracellular sodium ion (10–15 mmol/L and 140–150 mmol/L, respectively) result in low resolution (2–10 mm) and low signal-to-noise ratio (around 20–40) [9]. In light of all these, using SAM would be a very worthy addition for sodium concentration imaging and monitoring. In this paper, we claimed that time-dependent acoustic impedance measurements of sodium concentration activity using SAM with 80 MHz ultrasonic transducer with a lateral resolution of 20 μm has a vast amount of benefits over previously aforementioned sodium analysis methods. Over clinically proven sodium monitoring tools, the first advantage of SAM for imaging and monitoring of sodium ion dynamics is that it is relatively fast technique in which data acquisition of 2D acoustic impedance images with an area of 4.8 mm × 4.8 mm containing 300 × 300 sampling points takes about 2 min. Also, the attractiveness of SAM is that it offers micrometer resolution (around 20 μm at 80 MHz) alongside easy-to-perform and direct monitoring. Further, acoustic impedance measurement of sodium ion dynamics by SAM is a non-destructive monitoring tool whereas sodium assays measuring total cell sodium level such as flame photometry, atomic absorption spectrophotometry and neutron activation destroy the samples. Accordingly, the non-destructive nature of SAM is an advantage when the sample under investigation is desired to be used for following observations such as light microscopy analysis. Another advantageous property of SAM is the ease of sample preparation and hence it avoids inducing any mechanical changes in the samples due the specific sampling process (i.e staining or fixation) [26]. Thus, to overcome artifacts caused by alterations due to sample preparation, acoustic impedance measurement through SAM for the imaging and monitoring of sodium ion within biological media such as tissue, cell populations or serum may be useful. With this study, we showed that SAM shows a promise as a sodium monitoring tool.

In this investigation, we focused on monitoring of sodium diffusion since sodium is a vital component of living organisms and alterations in sodium ion homeostasis are known to be fundamental indicators of cautious complications in the integrity of ion and cellular balance. In light of this information, in future, the success of SAM in quantifying sodium concentration activity by time-dependent acoustic impedance measurements could be extended to the non-destructive, interference-free and easy-to-operate marker to follow dynamic processes such as the interaction of chemotherapy treatment with the tissue or cell populations *in vitro*.

5. Conclusion

The main aim of this work was to assess the applicability of time-varying acoustic impedance measurements by SAM in the quantification of the sodium diffusion. With this research, for the first time, we showed the ability of SAM to monitor time-dependent variations in acoustic impedance using NaCl diffusion in an agarose phantom. The results showed that SAM should be appropriate in future for determination of sodium and that this acoustic tool may be applied not only in obtaining static images but also utilized for dynamic investigations of sodium ion such as the interaction of chemotherapeutic agents with the tissue or cell populations.

Funding

This work was supported by grants from the Ministry of Development of Turkey (Project Number: 2009K120520) and Bogazici University Research Fund (Project Number: 11461).

References

[1] E. Murphy, D.A. Eisner, Regulation of intracellular and mitochondrial sodium in health and disease, Circ. Res. 104 (3) (2009) 292–303.
[2] A.M. Rose, R. Valdes, Understanding the sodium pump and its relevance to disease, Clin. Chem. 40 (9) (1994) 1674–1685.
[3] J.C. Skou, M. Esmann, The Na, K-atpase, J. Bioenerg. Biomembr. 24 (3) (1992) 249–261.
[4] A. Minta, Y. Tsien Roger, Fluorescent indicators for cytosolic sodium, J. Biol. Chem. 264 (32) (1989) 19449–19457.
[5] R.A. Garcia, C.P. Vanelli, O.D.S. Pereira Junior, J.O.D.A. Corra, Comparative analysis for strength serum sodium and potassium in three different methods: flame photometry, ionselective electrode (ISE) and colorimetric enzymatic, J. Clin. Lab. Anal. (2018) e22594.
[6] G.P. Amorino, M.H. Fox, Intracellular Na+ measurements using sodium green tetraacetate with flow cytometry, Cytometry: J. Int. Soc. Anal. Cytology 21 (3) (1995) 248–256.
[7] L.L. Hansen, J. Rasmussen, E. Friche, J.W. Jaroszewski, Method for determination of intracellular sodium in perfused cancer cells by 23Na nuclear magnetic resonance spectroscopy, Anal. Biochem. 214 (2) (1993) 506–510.
[8] J. van der Veen, P. Van Gelderen, J.H.N. Creyghton, W.M.M.J. Bovee, Diffusion in red blood cell suspensions: separation of the intracellular and extracellular NMR sodium signal, Magn. Reson. Med. 29 (4) (1993) 571–574.
[9] Madelin Guillaume, Ravinder R. Regatte, Biomedical applications of sodium MRI in vivo, J. Magn. Reson. Imaging 38 (3) (2013) 511–529.
[10] Andrew Briggs, An Introduction to Scanning Acoustic Microscopy, Oxford University Press, Royal Microscopical Society, 1985, pp. 1–70.
[11] K. Raum, K. Kempf, H.J. Hein, J. Schubert, P. Maurer, Preservation of microelastic properties of dentin and tooth enamel in vivo - a scanning acoustic microscopy study, Dent. Mater. 23 (10) (2007) 1221–1228.
[12] K. Kobayashi, S. Yoshida, Y. Saijo, N. Hozumi, Acoustic impedance microscopy for tissue characterization, Ultrasonics 54 (7) (2014) 1922–1928.
[13] S. Irie, K. Inoue, K. Yoshida, J. Mamou, K. Kobayashi, H. Maruyama, T. Yamaguchi, Speed of sound in diseased liver observed by scanning acoustic microscopy with 80 MHz and 250 MHz, J. Acoustical Soc. Am. 139 (1) (2016) 512–519.
[14] K. Ito, K. Yoshida, H. Maruyama, J. Mamou, T. Yamaguchi, Acoustic impedance analysis with high-frequency ultrasound for identification of fatty acid species in the liver, Ultrasound Med. Biol. 43 (3) (2017) 700–711.
[15] Y. Saijo, M. Tanaka, H. Okawai, F. Dunn, The ultrasonic properties of gastric cancer tissues obtained with a scanning acoustic microscope system, Ultrasound Med. Biol. 17 (7) (1991) 709–714.
[16] T. Kundu, J. Bereiter-Hahn, I. Karl, Cell property determination from the acoustic microscope generated voltage versus frequency curves, Biophys. J. 78 (5) (2000) 2270–2279.
[17] X. Zhao, R. Akhtar, N. Nijenhuis, S.J. Wilkinson, L. Murphy, C. Ballestrem, B. Derby, Multi-layer phase analysis: quantifying the elastic properties of soft tissues and live

cells with ultra-high-frequency scanning acoustic microscopy, IEEE Trans. Ultrason. Ferroelectrics Frequency Control 59 (4) (2012).
[18] K. Miura, H. Nasu, S. Yamamoto, Scanning acoustic microscopy for characterization of neoplastic and inflammatory lesions of lymph nodes, Sci. Rep. 3 (2013) 1255.
[19] K. Miura, S. Yamamoto, A scanning acoustic microscope discriminates cancer cells in fluid, Sci. Rep. 5 (2015) 15243.
[20] T.T.K. Soon, T.W. Chean, H. Yamada, K. Takahashi, N. Hozumi, K. Kobayashi, S. Yoshida, Effects of anticancer drugs on glia-glioma brain tumor model characterized by acoustic impedance microscopy, Jpn. J. Appl. Phys. 56 (7S1) (2017) 07JF15.
[21] J.R. Cook, R.R. Bouchard, S.Y. Emelianov, Tissue-mimicking phantoms for photoacoustic and ultrasonic imaging, Biomed. Opt. Express 2 (11) (2011) 3193–3206.
[22] S. Lee, H.Y. Lee, I.F. Lee, C.Y. Tseng, Ink diffusion in water, Eur. J. Phys. 25 (2) (2004) 331.
[23] J. Crank, The Mathematics of Diffusion, second ed., Clarendon Press, Oxford, 1975, pp. 1–32.
[24] M.J. Hamamura, L.T. Muftuler, O. Birgul, O. Nalcioglu, Measurement of ion diffusion using magnetic resonance electrical impedance tomography, Phys. Med. Biol. 51 (11) (2006) 2753.
[25] R.Gr. Maev, Acoustic Microscopy: Fundamentals and Applications, John Wiley and Sons, 2008, pp. 9–20.
[26] Ronald J. Barr, G.M. White, J.P. Jones, L.B. Shaw, P.A. Ross, Scanning acoustic microscopy of neoplastic and inflammatory cutaneous tissue specimens, J. Invest. Dermatol. 96 (1) (1991) 38–42.
[27] A.I. Gunawan, N. Hozumi, S. Yoshida, Y. Saijo, K. Kobayashi, S. Yamamoto, Numerical analysis of ultrasound propagation and reflection intensity for biological acoustic impedance microscope, Ultrasonics 61 (2015) 79–87.
[28] K. Zell, J.I. Sperl, M.W. Vogel, R. Niessner, C. Haisch, Acoustical properties of selected tissue phantom materials for ultrasound imaging, Phys. Med. Biol. 52 (20) (2007) N475.
[29] I.L. Cameron, N.K.R. Smith, T.B. Pool, R.L. Sparks, Intracellular concentration of sodium and other elements as related to mitogenesis and oncogenesis in vivo, Cancer Res. 40 (5) (1980) 1493–1500.
[30] R. Ouwerkerk, K.B. Bleich, J.S. Gillen, M.G. Pomper, P.A. Bottomley, Tissue sodium concentration in human brain tumors as measured with ^{23}Na MR imaging, Radiology 227 (2) (2003) 529–537.
[31] R.P. Kline, E.X. Wu, D.P. Petrylak, M. Szabolcs, P.O. Alderson, M.L. Weisfeldt, J. Katz, Rapid in vivo monitoring of chemotherapeutic response using weighted sodium magnetic resonance imaging, Clin. Cancer Res. 6 (6) (2000) 2146–2156.
[32] A.M. Babsky, H. Zhang, S.K. Hekmatyar, G.D. Hutchins, N. Bansal, Monitoring chemotherapeutic response in RIF-1 tumors by single-quantum and triple-quantum-filtered 23Na MRI, 1H diffusion-weighted MRI and PET imaging, Magn. Reson. Imaging 25 (7) (2007) 1015–1023.
[33] V.D. Schepkin, B.D. Ross, T.L. Chenevert, A. Rehemtulla, S. Sharma, M. Kumar, J. Stojanovska, Sodium magnetic resonance imaging of chemotherapeutic response in rat glioma, Magn. Reson. Med. 53 (1) (2005) 85–92.
[34] D. Fanelli, A.J. McKane, G. Pompili, B. Tiribilli, M. Vassalli, T. Biancalani, Diffusion of two molecular species in a crowded environment: theory and experiments, Phys. Biol. 10 (4) (2013) 045008.
[35] D. Bhatnagar, D. Joshi, A. Kumar, C.L. Jain, Direct acoustic impedance measurements of dimethyl sulphoxide with benzene, carbon tetrachloride and methanol liquid mixtures, Indian J. Pure Ap. Phy. 48 (1) (2010) 31–35.
[36] A.H. Muhr, J.M. Blanshard, Diffusion in gels, Polymer 23 (7) (1982) 1012–1026.
[37] E.J. Schantz, A.M. Lauffer, Diffusion measurements in agar gel, Biochemistry 1 (4) (1962) 658–663.